ACS APPLIED MATERIALS & INTERFACES

Research Article

www.acsami.org

Porous Polyurea Network Showing Aggregation Induced White Light Emission, Applications as Biosensor and Scaffold for Drug Delivery

Subhajit Bhunia,[†] Nabanita Chatterjee,[‡] Subhadip Das,[‡] Krishna Das Saha,[‡] and Asim Bhaumik*[,†]

[†]Department of Material Science, Institution Association for the Cultivation of Science, Jadavpur, Kolkata 700032, India

[‡]Cancer Biology and Inflammatory Disorder Division, CSIR-Indian Institute of Chemical Biology, Jadavpur, Kolkata 700032, India

Supporting Information

ABSTRACT: We have designed a urea functionalized novel nanoporous material, POP-PU, which showsaggregation induced white light emission in the presence of suitable polar solvents. This nanomaterial has been explored as a pseudowhite light emitter where the polymeric luminogen moiety can interact with the suitable polar solvent, leading to charge transfer. Thus, solvent assisted rotational freezing of nonrigid polymeric nanoparticles gives radiative emission and the whole solution emits white light with color temperature of 8533 K. This nanoporous material also holds the pockets (donor−donor−acceptor array) for specific biomolecular interaction. Among three pyrimidine based nucleotide bases, only cytosine can amplify the PL emission intensity of POP-PU and the other two bases cannot, suggesting its future potential as a biosensor. Further, this urea functionalized porous organic nanomaterial can be utilized as an efficient drug-delivery vehicle for liver cancer diagnostics and therapy based on the specific biomolecular interaction at its surface.

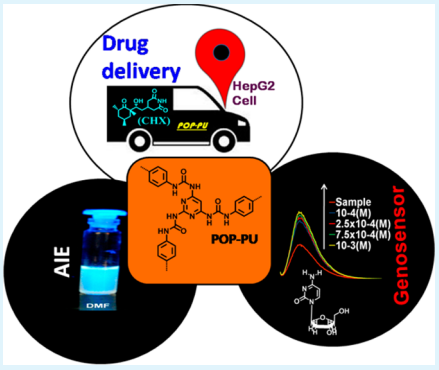

KEYWORDS: *biosensor, drug delivery, organic white light emitter, polyurea network, porous organic polymer*

INTRODUCTION

Responsive polymeric materials, which can form supramolecular nanostructures in the presence of external stimuli, have attracted increasing interest over the years due to their diverse range of desired applications, such as drug delivery, diagnostics, "smart" optical systems, biosensors and so on.[1] Among the polymers, porous organic polymers (POPs),[2−9] which combine the surface porosity of the material and reactive organic functional groups of the framework are a rapidly developing class of materials due to their tunability of pore aperture and the diversity of functional groups that could present in the framework building blocks. POPs are typically prepared through polymerization/condensation,[10−12] cyclization[13] or metal mediated coupling/addition or solvothermal reactions.[14−16] Although the organic functional groups present in these POPs are mostly utilized for gas storage and catalytic applications,[17,18] their specific interaction with solvent molecules, leading to solvatochromic behavior, gelation, aggregation induced emission,[19] biosensing and related biomedical applications, have not been explored so far. However, there are hardly any reports on porous organic polymers, which could show aggregation induced white light emission in the presence of a solvent.

Genosensors or nucleic acid probe based biosensors, which utilize the interaction of the nucleic acid with the ligand binding sites, are very important for genome mapping and gene sequence analysis.[20] If phenyl and pyrimidine nuclei are interconnected through urea (-NHCONH-) functionality, the resulting polyurea network bearing the DDA (donor−donor−acceptor) array can interact via hydrogen bonding to enhance binding affinity to a complementary AAD array and may cause photoluminescence signal amplification for the nucleotide bases.[21,22] In this context, it is pertinent to mention that porous organic polymers have not been explored in theranostics for anticancer drugs. Such nanotechnological advancement is highly desired in the pharmaceutical and drug industry.[23] Mesoporous silica, metal oxides, metal organic frameworks (MOFs) and many organic polymeric micelles have been employed for controlled drug delivery in recent times.[24,25] From the inorganic platform gold, platinum nanoparticles are most effective drug delivery carrier due to their inertness. However, their nonbiodegradability is often a serious issue when accumulated in the human body. From the viewpoint of cost and biodegradability organic polymeric nanoparticles are superior than inorganic metal and ceramic nanoparticles. Although, organic liposomal drug delivery is a clinically established method but it has serious drawbacks like low encapsulation efficiency, fast release of drugs, poor storage stability and lack of tunable triggers for drug release.[26] Organic polymeric nanoparticles such as polylactide−polyglycolide copolymers, polyacrylates and polycaprolactones are other smart nanosystems known for drug delivery due to the change in their physicochemical properties in response to environmental signals and their biodegradability. However, these

Received: September 29, 2014
Accepted: December 2, 2014
Published: December 2, 2014

systems are devoid of any biosensing or white light emission properties.

Herein, we first report the synthesis of a pyrimidine containing urea functionalized porous organic polymer material, POP-PU, through the organic sol–gel reaction of 2,4,6-triaminopyrimidine and 1,4-phenylene diisocyanate followed by agglomeration to obtain the pyrimidyl urea network material,[27] which showed a solvent-dependent white light emission property. Addition of an excess amount of nonsolvent to the sol produced, through the reaction between 2,4,6-triaminopyrimidine and 1,4-phenylene diisocyanate, the organic nanomaterial POP-PU (Figure 1). Here we have shown a new

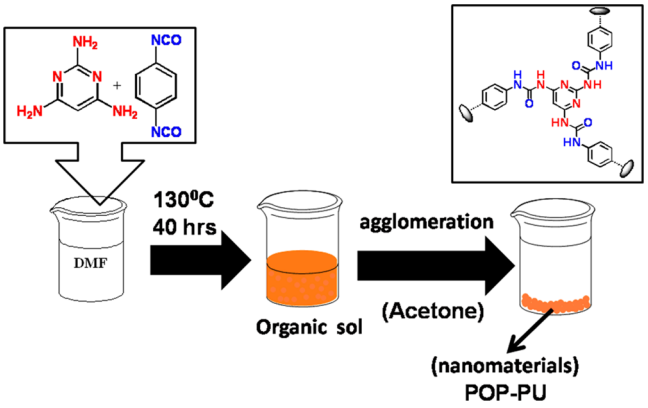

Figure 1. Reaction of 2,4,6-triaminopyrimidine and 1,4-phenylene diisocyanate under organic sol–gel conditions and agglomeration at the nanoscale to produce POP-PU.

nanoporous organic biodegradable polyurea network obtained from a simple one-step synthetic process that can be used as an excellent carrier for drug delivery and simultaneously enhances the efficiency of the anticancer drug and liver cancer therapeutics. Due to the presence of the DDA array in POP-PU, it can interact strongly with cycloheximide, which could facilitate its potential as a drug-delivery carrier. Further, the fluorescence property of POP-PU suggests promising biomedical applications, especially the intervention of the theranostics approach in liver cancer prevention.[28,29] The "apoptotic trigger" in cancer cells is considered as the keynote phenomenon in cancer therapy.[30,31] Considering all these unique features, we have explored the three-in-one application potentials of the novel multifunctional material POP-PU as (i) a white light emitter, (ii) a genosensor for the nucleotide base cytosine and (iii) a drug-delivery vehicle for the liver cancer diagnostics and therapy using cycloheximide as a model drug.

RESULT AND DISCUSSION

The Fourier transform infrared spectroscopy (FTIR) absorption band at 1632 cm^{-1} for POP-PU could be attributed to the C═O stretching frequency, whereas the 3299 and 1220 cm^{-1} bands are assigned due to the N—H and C—N stretching frequencies, as shown in Figure 2a. Absence of a peak corresponding to the primary $-NH_2$ group in the FTIR spectrum of POP-PU suggested complete condensation between the amine and isocyanate groups in this POP-PU network. The chemical environments of different carbon atoms of the constituent moieties of the POP-PU framework have been analyzed from the respective solid state ^{13}C CP MAS NMR spectrum, as shown in Figure 2b. POP-PU showed

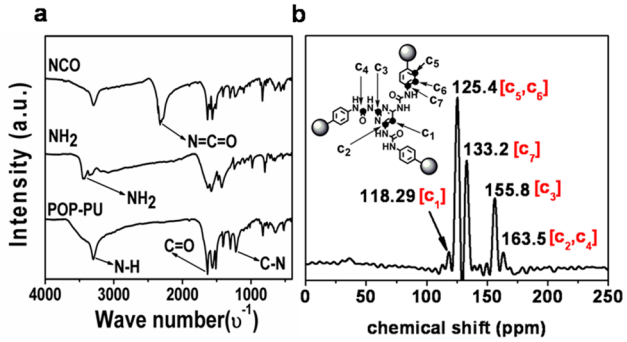

Figure 2. (a) FTIR spectra of 2,4,6-triaminopyrimidine, 1,4-phenylene diisocyanate, POP-PU and (b) ^{13}C solid state CP MAS NMR spectrum of POP-PU.

strong signals corresponding to the presence of phenyl (C_5, C_6 and C_7) and pyrimidine (C_1, C_2 and C_4) rings, and these are interconnected through urea group (C_3). The N_2 adsorption/desorption isotherms at 77 K for POP-PU follow the type IV isotherm (Figure 3) together with a noticeable desorption

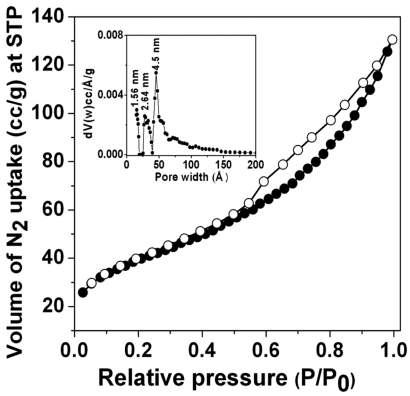

Figure 3. N_2 adsorption/desorption isotherms of POP-PU nanomaterial. Adsorption points are marked by filled circles and desorption points by empty circles. (Inset) pore size distribution employing the NLDFT method.

hysteresis loop corresponding to random mesopores. The Brunauer–Emmett–Teller (BET) surface area of the POP-PU is 142 $m^2\ g^{-1}$. The pore size distribution of POP-PU, using the nonlocal density functional theory (NLDFT) and carbon slit pore model, suggested a trimodal porosity with peaks at 1.5, 2.8 and 4.5 nm (Figure 3, inset). From the nature of the adsorption isotherm, mesoporosity in the POP-PU material is quite evident. The X-ray diffraction pattern of POP-PU is shown in Figure S1 (Supporting Information), where one broad peak at 2θ = 2.2°, corresponding to a disordered mesophase, is observed. Further, sharp peaks at 2θ = 11.9, 20.6, and 21.6° suggested a semicrystalline nature of the polymeric network of POP-PU (inset of Figure S1, Supporting Information).

High resolution transmission electron microscopy (HRTEM) images of the POP-PU material obtained via nonsolvent induced agglomeration are shown in Figure 4. From these images, it is clear that POP-PU possesses a hair-like nanofiber morphology, having hair lengths of ca. 75–140 nm and a width of ca. 5 nm. These nanofibers are uniformly distributed throughout the specimen grid. The internal void spaces between the nanoparticles could be the origin of a wide range of porosities (supermicropores to mesopores) in POP-

dx.doi.org/10.1021/am5066859 | ACS Appl. Mater. Interfaces 2014, 6, 22569–22576

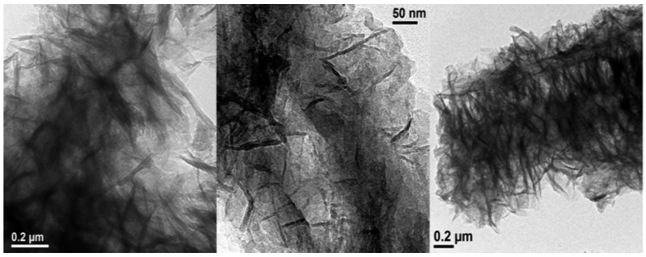

Figure 4. HRTEM images of POP-PU nanofibers at different magnifications.

PU. It is pertinent to mention that a nanoporous organic polymer with white light emission in the aggregate or solid state is rare because aggregation of a polymer generally quenches light emission. Here this new polyurea network of POP-PU bearing a pyrimidine and phenylene ring has been generated through the reaction of the amine and isocyanate groups. A large amount of acetone was added as a nonsolvent to prepare the organic sol and to agglomerate the particles to the nanoscopic range (75−140 nm). The material is virtually nonluminiscent in the solid state but the diluted solution of POP-PU in dimethylformamide (DMF) generates the white light emission property. The intrinsic photoluminescence of POP-PU in water under ultraviolet excitation (at 378 nm) showed strong emission at wavelengths between 390 and 520 nm. The most compulsive fact is that the nonfluorescent material transforms to a bluish-white light emitter in DMF with the CIE coordinate (0.26, 0.38) and the color temperature (8533 K). The corresponding photoluminescence spectrum is shown in Figure 5b. It shows three humps at 433, 484 and 532

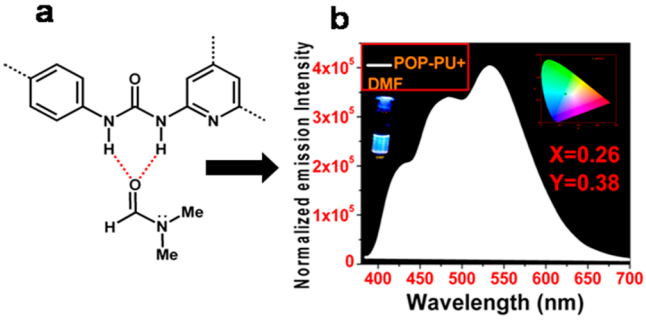

Figure 5. (a) Strong H-bonding interactions between POP-PU and DMF, (b) PL spectrum of POP-PU+DMF and CIE coordinate (exitation at 378 nm).

nm, suggesting the white color is a three color white. This type of radiative emission is attributed to the fact, DMF assisted freezing of single-bond rotational freedom of the urea functionalized network (Figure 5a). PL spectra in $CHCl_3$ and acetone showed very poor emission, whereas emission intensity was drastically amplified in dimethyl sulfoxide (DMSO), DMF and ethanol (EtOH) (Figure 6a). Respective photographs are shown in Figure 6b. The enthalpy of interaction of urea with DMF and similar solvents like DMAc is exceptionally larger than those of other solvents.[32] So, the conformationally flexible network is rigidified in DMF and DMAc to a greater extent, as the nonradiative energy loss due to flexibility of bond rotation is restricted abruptly in DMF and DMAc. So, the intrinsic nonfluorescent nanofiber gains the white light emitting property in the solution phase. A high concentration of the

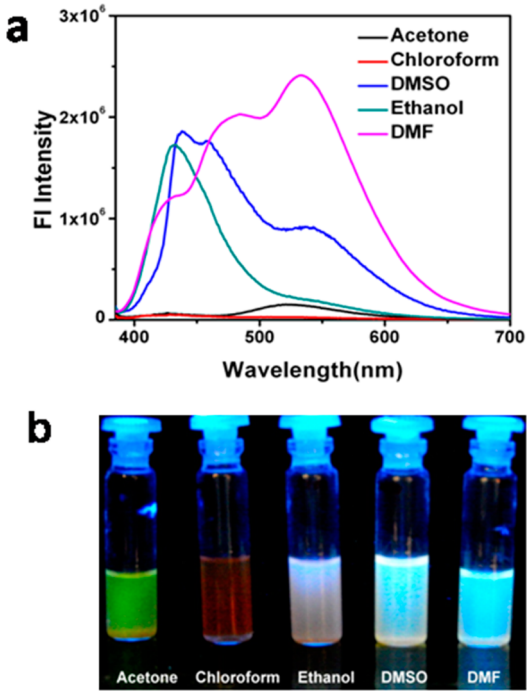

Figure 6. (a) PL spectra of POP-PU material in different solvent (excitation at 375 nm) (b) photographic images of POP-PU in different solvents after photoexcitaton.

individual building blocks in POP-PU in the presence of DMF solvent resulted in a supramolecular polymeric assembly via charge-transfer (Figure S2, Supporting Information).[33,34] A considerable increase in average particle size vis-à-vis that in water suggested aggregation of POP-PU in DMF. Thus, this porous polymer backbone may be rigidified by virtue of a series of hydrogen bonds between the urea moiety[35,36] and the solvent molecules (Figure 5a), leading to restriction of the intramolecular rotation, and the material behaves like a solid-state luminogen to cause aggregation-induced emission (AIE).[37] The restricted geometries of the donor and acceptor moieties of POP-PU in the presence of DMF solvent could induce physical constraints in the supramolecular polymeric backbone, which minimize the nonradiative energy losses of their excitons and maximize their probability of radiative transitions, leading to white light emission. This property is prominent in DMF.[38−40] Thus, although the building blocks in solvents are nonemissive, the network polymers are highly luminescent in various solvents and such three color white light emitters based on metal-free porous polymeric material are very desired.

POP-PU as Biosensing of Cytosine. Further, POP-PU has functionality containing an appropriate hydrogen bonding array (donor−donor−acceptor) in the framework, thus we have examined it's possibility for recognizing cytosine (Figure 7a), an important hydrogen bonding unit for DNA binding. The binding between cytosine and POP-PU has been studied by taking photoluminescence spectra of the same amount of POP-PU sample in different concentrations of aqueous solutions of cytosine. As seen from the figure, a large enhancement of PL intensity is observed with increasing the concentration of cytosine.[41,42] The experiment has also been carried out using the other pyrimidine bases thymine and uracil. But for the last two cases, significant decreases in PL intensity are observed (Figure 7b,c). It is pertinent to mention that the photo-

dx.doi.org/10.1021/am5066859 | ACS Appl. Mater. Interfaces 2014, 6, 22569−22576

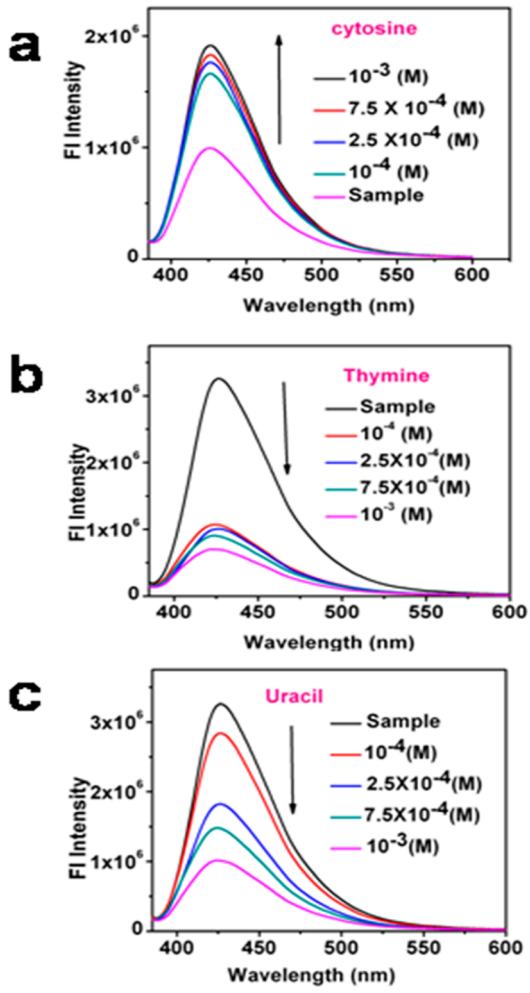

Figure 7. Photoluminescent spectra of (a) cytosine–POP-PU (amplifying); (b) thymine–POP-PU (quenching) and (c) uracil–POP-PU (quenching). Two milliliters 0.04 wt % aqueous solution of POP-PU was used for all the analyses. Excitation wavelength was 378 nm.

luminescence spectrum of only cytosine suggests that cytosine is totally nonfluorescent. Thus, the enhancement of PL intensity is not due to fluorescence from cytosine. Biosensors based on mesoporous materials are very desirable today.[43] Thus, POP-PU can act as a solid-state biosensor for the selective sensing of cytosine when it is present along with the three pyrimidine based nucleotide bases. Because the functional architecture of the POP-PU material holds the pocket to interact with nucleotide bases, this material can be employed as a nanocarrier for drug delivery. The nucleotide bases interact with the material through complementary H-bonded interactions. So, the drug molecules like cytarabine, cycloheximide, etc., which have the resemblance of a structure with nucleotide bases, can undergo complementary H-bonding with the tris (urea)pyrimidine moiety of the host material (Figure 8a). On the basis of such interactions, we have explored the POP-PU material as a drug delivery vehicle using cycloheximide, a well-known protein synthesis inhibitor, as a model drug in the following section.

POP-PU as Drug Delivery vehicle for Cycloheximide. The presence of H-bond donor and acceptor sites in close vicinity in POP-PU has been explored for their capability of binding with many anticancer drugs (cytarabine) and protein

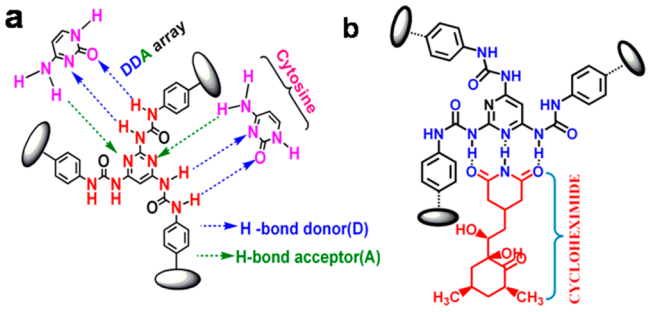

Figure 8. (a) Interaction of cytosine with POP-PU having DDA array (left). (b) Possible H-bonding interaction between POP-PU and protein biosynthesis inhibitor (cycloheximide, right).

synthesis inhibitors (cycloheximide) and thus can be used as a nanocarrier.[44,45] We have shown the possible interaction between cycloheximide (model anticancer drug) and the POP-PU material (Figure 8b). To trigger the apoptotic efficacy, cycloheximide loaded POP-PU (POP-PU-CHX) (0–0.02 nM) was evaluated for its cytotoxic property in cancer cells (Figure 9a). However, the POP-PU was not effective to elicit any

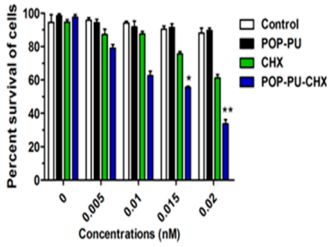

Figure 9. Cells were treated with POP-PU in the concentration range (0–0.02 nM) of CHX, POP-PU-CHX for 36 h. The significance result was found with POP-PU-CHX as compared to CHX.

significant cytotoxicity. The results of cell cytotoxicity assay indicated that there was no variation for two different type cells, normal cells and cancerous cells, with POP-PU only. POP-PU-CHX reduced the viability of $HepG_2$ cells with GI50 values of 0.01256 ± 0.00344 considerably after 36 h, in comparison with only cyclohexamide.

Mitochondrial integrity or the loss of membrane potential (Ψ_m) has been linked to the initiation and activation of the series of apoptotic cascade with synchronized release of cytochrome c. Fluorescence emission shift of the Ψm sensitive cationic JC-1 dye. Cells were treated with 0.02 nM POP-PU-CHX and stained with JC-1; cells showed potential depolarization of the mitochondrial membrane. Detailed biological studies on POP-PU are illustrated in the Supporting Information, section S1 and Figures S3–S6.

Nanomedicine. *Apoptosis Inducing Effect of Cycloheximide Loaded POP-PU.* For triggering the apoptotic efficacy, cycloheximide loaded POP-PU (POP-PU-CHX) (0–0.02 nM) was evaluated for its cytotoxic property in cancer cells (Figure S3, Supporting Information). However, the POP-PU was not effective to elicit any significant cytotoxicity. The results of the cell cytotoxicity assay indicated that there was no variation for the two different types of cells, normal cells and cancerous cells, with POP-PU only (Figure S3, Supporting Information). To confirm the apoptosis induction effect against cancer cells afforded by the POP-PU-CHX, annexin-PI cytometry assay was conducted in $HepG_2$ cells. POP-PU-

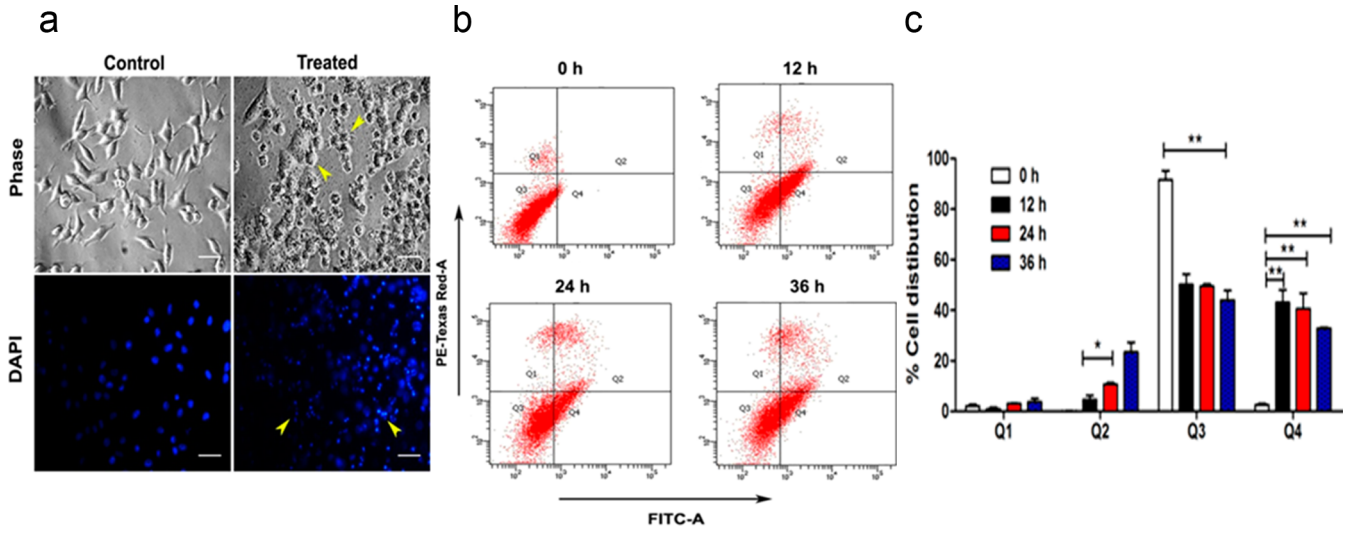

Figure 10. (a) Morphological changes observed in HepG2 cells after 0.02 nM POP-PU-CHX treatment for 36 h and shown under fluorescence microscopy after DAPI staining (scale bar 10 μm). (b) Annexin V-FITC binding in HepG2 cells at different times including 0, 12, 24 and 36 h. The data are represented as mean ± SEM (*P < 0.05, **P < 0.01) of triplicate independent experiments. (c) Effect of POP-PU-CHX on Annexin V-FITC binding in HepG2 cells at different times including 0, 12, 24 and 36 h, and denotations like Q1, Q2, Q3 and Q4 are identified as necrotic cells, late apoptotic cells, live cells and apoptotic cells. The data are represented as mean ± standard error of the mean (SEM) from triplicate independent experiments.

CHX rapidly reduced the viability of the $HepG_2$ cells with GI50 values of 0.01256 ± 0.00344 after 36 h, in comparison with only cyclohexamide channelized in $HepG_2$ cells, which geared up the release of annexin from the cell membrane and afforded apoptosis, as shown in Figure 10b. An intercellular instance of phosphatidyl serine exposure was sequentially correlated with nuclei fragmentation stained with DAPI, as evident from Figure 10a. The reflection of apoptosis also was found in cell cycle arrest (Figure 11) in the treatment of the cells with 0.02 nM

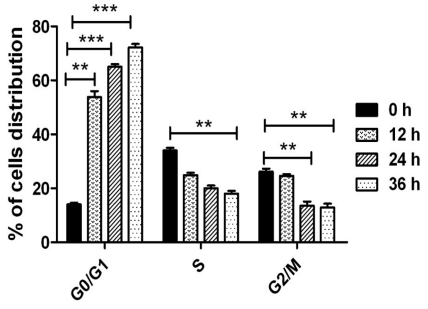

Figure 11. Cell cycle analysis up to 36 h with the concentration of 0.02 nM. The data are represented as mean ± SEM (*P < 0.05, **P < 0.01) of triplicate independent experiments.

POP-PU-CHX for 0, 12, 24 and 36 h. This study confirms that POP-PU-CHX induces apoptosis in $HepG_2$ cells at lower concentrations than cycloheximide alone.

Cellular Uptake Study with Cycloheximide Loaded on POP-PU. Cellular uptake studies were performed to ascertain the internalization of POP-PU-CHX in $HepG_2$ cells. Florescence images (Figure 12a) revealed the localization of POP-PU-CHX within the cytosolic region of the cells at a concentration of 0.02 nM in 36 h, which simultaneously instantiated the fluorophore property and resulted in cellular apoptosis. The accumulation of POP-PU-CHX (0.02 nM) was also evidenced and confirmed in $HepG_2$ cells as time-dependent through Flow cytometry (FACS) analysis (Figure 12b). These results suggested that POP-PU-CHX may be explored as novel compound by generating excessive ROS which is one of the potent cause to induce apoptosis leading to cell death through the damage of cellular protein, lipid and DNA. The molecular approach of a fluorophore in POP-PU-CHX having the cell detecting properties together with its therapeutic intervention is very challenging in the context of cancer research.

Effect of POP-PU-CHX in Mitochondrial Membrane Potential with Cytochrome c and Caspases. Photostable AIE luminogens have been employed for mitochondrial imaging and tracking. Mitochondrial integrity or the loss of membrane potential (Ψ_m) has been linked to the initiation and activation of the apoptotic cascade with synchronized release of cytochrome c.[46] We have investigated whether POP-PU-CHX would be able to generate oxidative stress by means of measuring reactive oxygen species (ROS) in spectrofluorimetric analysis. As shown in Figure S5 (Supporting Information), we found POP-PU-CHX (0.02 nM) significantly induced a huge amount of ROS in $HepG_2$ cells in 36 h. Thus, the galvanized process precedes the apoptotic sequential occurrence including loss of mitochondrial membrane potential (Ψ_m) and increase of cytosolic cytochrome c release that altered the pro- and antiapoptotic protein levels with simultaneous activation of the caspase series. To determine whether POP-PU-CHX induced apoptosis in $HepG_2$ cells involves mitochondrial disruption, we have examined the depolarization of mitochondrial membrane by measuring the fluorescence emission shift of the Ψ_m sensitive cationic JC-1 dye is observed. Cells were treated with 0.02 nM POP-PU-CHX and stained with JC-1; cells showed the potential depolarization of mitochondrial membrane (Figure 12c). A significant increment of cytochrome c release in the cytosolic portion (Figure S6A, Supporting Information) was balanced with a reduced amount in the mitochondrial portion (Figure S6B, Supporting Information) in $HepG_2$ cells, as quantified by ELISA. Generation of excessive ROS is one of the potent causes to induce apoptosis, leading to cell death through the damage of cellular proteins. Therefore,

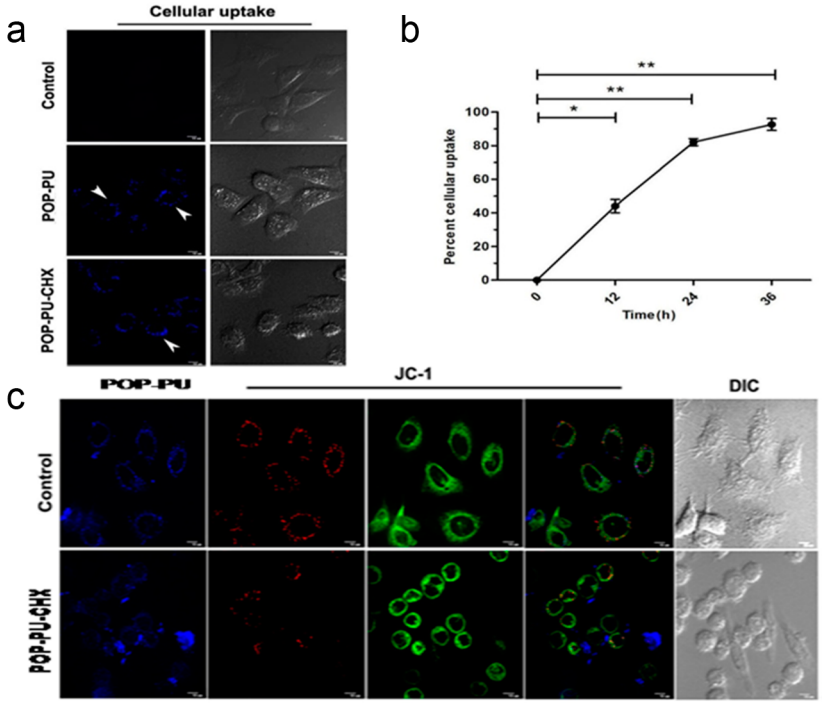

Figure 12. (a) Effect of POP-PU-CHX on HepG2 cells and cell imaging by POP-PU-CHX at concentration of 0.02 nM treatment using confocal laser microscopy with accurate laser. Scale bar 10 μm. (b) Cellular uptake studies: % cellular uptake of POP-PU-CHX by HepG2 cells with increasing time (h) spectrofluorimetric analysis. (c) Effect of POP-PU-CHX on $HepG_2$ cells on membrane potential evaluated with JC-1 dye reactively by confocal imaging.

POP-PU-CHX elicited the activation of initiator caspase 9 and effectors of caspase 3 in HepG2 cells, as shown in Figure S6C (Supporting Information). These results indicate that POP-PU-CHX induces the cellular apoptosis via a ROS mediated mitochondrial pathway.

EXPERIMENTAL SECTION

Powder X-ray diffraction (XRD) patterns of POP-PU samples were analyzed with a Bruker D8 Advance X-ray diffractometer using Ni-filtered Cu Kα (λ = 0.154 06 nm) radiation. N_2 adsorption–desorption isotherms were recorded on an Autosorb 1C (Quantachrome Instruments, USA) at 77 K. High resolution transmission electron microscopy (HRTEM) images of the porous polymers were obtained using a JEOL JEM 2010 transmission electron microscope operating at 200 kV voltage. The UV–vis spectrum of POP-PU was recorded on a Shimadzu UV-2401PC doubled beam spectrophotometer having an integrating sphere attachment for solid samples. Photoluminescence spectra of the POP-PU in were taken in a Horiba fluorolog 3. Carbon, hydrogen and nitrogen contents were determined by a PerkinElmer 2400 Series II CHN analyzer.

1. Materials. 2,4,6-Triaminopyrimidine and 1,4-phenylene diisocyanate were procured from Sigma-Aldrich, and anhydrous DMF was obtained from Spectrochem, India. Other reagents are purchased from Merck, India.

Synthesis of POP-PU Nanopowder. The synthesis of POP-PU was carried out by the sol–gel microemulsion technique to obtain the nanoscopic organic material. 250 mg (2 mmol) of 2,4,6-triaminopyrimidine and 480 mg (3 mmol) of 1,4-phenylene diisocyanate were refluxed in 35 mL of anhydrous DMF at 428 K under N_2 atmosphere for 2 days. The reaction mixture was cooled to room temperature, which gave an orange colored suspension. Then the polymeric nanoparticles were obtained by the agglomeration technique. 350 mL of acetone (nonsolvent) was poured into reaction mixture, and the solution was stirred for 1 h. The turmeric color precipitate was collected through vacuum filtration and successively washed with acetone, ethanol, tetrahydrofuran (THF) and methanol. The obtained powder material was dried at 353 K under vacuum to obtain POP-PU. The yield is 54% (400 mg) based on 2,4,6-triaminopyrimidine and 1,4-phenylene diisocyanate. Elemental analysis found by combustion: C, 51.9%; H, 5.40%; N, 24.53%. Calcd theoretical formula from an infinite POP-PU framework $[C_{25}H_{22}N_8O_3]_n$: C, 62.23%; H, 4.6%; N, 23.22%.

Genosensing Application. 20 mg of POP-PU sample was sonicated in 20 mL of deionized water for 1 h. Then that stock solution was added (1 mL) to each cuvette containing nucleotide bases of different concentrations prepared in deionized water. The experiment had been carried out for three different pyrimidine nucleotide bases: thymine, uracil and cytosine. Each time, the excitation wavelength was 378 nm.

In Vitro Cell Imaging and Cellular Uptake Studies. Cell imaging studies were carried out using the $HepG_2$ cell line, which was maintained in proper cell culture conditions. To study the cellular uptake of POP-PU-CHX, cells (1×10^4/well) were grown on 30 mm Petri dish well plates for 24 h at 37 °C and 5% CO_2 followed by incubation with POP-PU-CHX in cell culture medium for 36 h. After fixation, cells were acquired by confocal laser scanning (Revolution XD Spinning Disk with an iXon 897 EMCCD camera; Andor, Belfast, UK) after 36 h of incubation; cellular uptake study revealed that POP-PU-CHX was internalized by the cell membrane, leading to the cytosolic portions of the cells. Cellular uptake experiments were conducted according to a literature method with some modifications. After exposure to 0.02 nM POP-PU-CHX for 12, 24 and 36 h, the cells were taken and uptake study was performed by FACS analysis (BD LSRFortessa). For the details of the experiments employed for the cell culture, MTT assay, fluorescence imaging, changes in the mitochondrial membrane potential, estimation of intracellular ROS and the caspase 3, caspase 9 and cytochrome c assay, please see the Supporting Information.

CONCLUSIONS

A new porous polyurea based nanomaterial has been synthesized through organic sol–gel reaction between 2,4,6-

triaminopyrimidine and 1,4-phenylene diisocyanate followed by nonsolvent induced aggregation. The resulting porous polymer showed a high BET surface area, mesoporosity and solvent induced white light emission. This novel material has been explored in three frontline areas of energy and biomedical research: (i) pseudowhite light emitter due to solvent induced aggregation, (ii) selective biosensing of cytosine and (iii) high efficacy as a drug-delivery vehicle for therapy and diagnostics of cancer drug cycloheximide due to the presence of fluorophore moiety, nanoscale porosity and intrinsic binding sites, suggesting its future potential in energy and biomedical research.

■ ASSOCIATED CONTENT

Supporting Information

Small angle PXRD and corresponding wide angle PXRD of POP-PU, aggregation of POP-PU in DMF and water by dynamic light scattering study, and characterization, description and data interpretation of biological studies over nanoporous POP-PU. This material is available free of charge via the Internet at http://pubs.acs.org.

■ AUTHOR INFORMATION

Corresponding Author

*A. Bhaumik. E-mail: msab@iacs.res.in.

Notes

The authors declare no competing financial interest.

■ ACKNOWLEDGMENTS

S.B. thanks CSIR, New Delhi for a Junior Research Fellowship. A.B. thanks DST, New Delhi for DST-SERB project grant. The authors are thankful to Dr. S.N. Bhattacharya and Mr. D. Sarkar for confocal microscopy. K.D.S. thanks Prof. S. Roy, the Director CSIR-IICB and CSIR for necessary support.

■ REFERENCES

(1) Stuart, M. A. C.; Huck, W. T. S.; Genzer, J.; Müller, M.; Ober, C.; Stamm, M.; Sukhorukov, G. B.; Szleifer, I.; Tsukruk, V. V.; Urban, M.; Winnik, F.; Zauscher, S.; Luzinov, I.; Minko, S. Emerging Applications of Stimuli-Responsive Polymer Materials. *Nat. Mater.* **2010**, *9*, 101−113.

(2) Côté, A. P.; Benin, A. I.; Ockwig, N. W.; O'Keeffe, M.; Matzger, A. J.; Yaghi, O. M. Porous, Crystalline, Covalent Organic Frameworks. *Science* **2005**, *310*, 1166−1170.

(3) Chandra, D.; Jena, B. K.; Raj, C. R.; Bhaumik, A. Functionalized Mesoporous Cross-Linked Polymer as Efficient Host for Loading Gold Nanoparticles and Its Electrocatalytic Behavior for Reduction of H_2O_2. *Chem. Mater.* **2007**, *19*, 6290−6296.

(4) Uribe-Romo, F. J.; Hunt, J. R.; Furukawa, H.; Klöck, C.; O'Keeffe, M.; Yaghi, O. M. A Crystalline Imine-Linked 3-D Porous Covalent Organic Framework. *J. Am. Chem. Soc.* **2009**, *131*, 4570−4571.

(5) Dawson, R.; Laybourn, A.; Clowes, R.; Khimyak, Y. Z.; Adams, D. J.; Cooper, A. I. Functionalized Conjugated Microporous Polymers. *Macromolecules* **2009**, *42*, 8809−8816.

(6) Rabbani, M. G.; El-Kaderi, H. M. Template-Free Synthesis of a Highly Porous Benzimidazole-Linked Polymer for CO_2 Capture and H_2 Storage. *Chem. Mater.* **2011**, *23*, 1650−1653.

(7) Modak, A.; Mondal, J.; Bhaumik, A. Porphyrin based Porous Organic Polymers: Novel Synthetic Strategy and Exceptionally High CO_2 Adsorption Capacity. *Chem. Commun.* **2012**, *48*, 248−250.

(8) Thiel, K.; Zehbe, R.; Roeser, J.; Strauch, P.; Enthaler, S.; Thomas, A. A Polymer Analogous Reaction for the Formation of Imidazolium and NHC based Porous Polymer Networks. *Polym. Chem.* **2013**, *4*, 1848−1856.

(9) Kang, N.; Park, J. H.; Ko, K. C.; Chun, J.; Kim, E.; Shin, H. W.; Lee, S. M.; Kim, H. J.; Ahn, T. K.; Lee, J. Y.; Son, S. U. Tandem Synthesis of Photoactive Benzodifuran Moieties in the Formation of Microporous Organic Networks. *Angew. Chem., Int. Ed.* **2013**, *52*, 6228−6232.

(10) Bhunia, M. K.; Das, S. K.; Pachfule, P.; Banerjee, R.; Bhaumik, A. Nitrogen-Rich Porous Covalent Imine Network (CIN) Material as an Efficient Catalytic Support for C−C Coupling Reactions. *Dalton Trans.* **2012**, *41*, 1304−1311.

(11) Katsoulidis, A. P.; Kanatzidis, M. G. Mesoporous Hydrophobic Polymeric Organic Frameworks with Bound Surfactants. Selective Adsorption of C_2H_6 versus CH_4. *Chem. Mater.* **2012**, *24*, 471−479.

(12) Modak, A.; Pramanik, M.; Inagaki, S.; Bhaumik, A. A Triazine Functionalized Porous Organic Polymer: Excellent CO_2 Storage Material and Support for Designing Pd Nanocatalyst for C−C Cross-Coupling Reactions. *J. Mater. Chem. A* **2014**, *2*, 11642−11650.

(13) Islamoglu, T.; Rabbani, M. G.; El-Kaderi, H. M. Impact of Post-Synthesis Modification of Nanoporous Organic Frameworks on Small Gas Uptake and Selective CO_2 Capture. *J. Mater. Chem. A* **2013**, *1*, 10259−10266.

(14) Cheng, G.; Hasell, T.; Trewin, A.; Adams, D. J.; Cooper, A. I. Soluble Conjugated Microporous Polymers. *Angew. Chem., Int. Ed.* **2012**, *51*, 12727−12731.

(15) Lee, D.; Zhang, C. Y.; Wei, C.; Ashfeld, B. L.; Gao, H. F. Hierarchically Porous Materials *via* Assembly of Nitrogen-Rich Polymer Nanoparticles for Efficient and Selective CO_2 Capture. *J. Mater. Chem. A* **2013**, *1*, 14862−14867.

(16) Kubo, S.; White, R. J.; Tauer, K.; Titirici, M. M. Flexible Coral-like Carbon Nanoarchitectures via a Dual Block Copolymer−Latex Templating Approach. *Chem. Mater.* **2013**, *25*, 4781−4790.

(17) Moon, S.-Y.; Bae, J.-S.; Jeon, E.; Park, J.-W. Organic Sol−Gel Synthesis: Solution-Processable Microporous Organic Networks. *Angew. Chem., Int. Ed.* **2010**, *49*, 9504−9508.

(18) Suresh, V. M.; Bonakala, S.; Atreya, H. S.; Balasubramanian, S.; Maji, T. K. Amide Functionalized Microporous Organic Polymer (AmMOP) for Selective CO_2 Sorption and Catalysis. *ACS Appl. Mater. Interfaces* **2014**, *6*, 4630−4637.

(19) Liu, Y.; Tao, X.; Wang, F.; Dang, X.; Zou, D.; Ren, Y.; Jiang, M. Aggregation-Induced Emissions of Fluorenonearylamine Derivatives: A New Kind of Materials for Nondoped Red Organic Light-Emitting Diodes. *J. Phys. Chem. C* **2008**, *112*, 3975−3981.

(20) Beattie, K. L.; Beattie, W. G.; Meng, L.; Turner, S. L.; Coral-Vazquez, R.; Smith, D. D.; McIntyre, P. M.; Dao, D. D. Advances in Genosensor Research. *Clin. Chem.* **1995**, *41*, 700−706.

(21) Abbel, R.; Grenier, C.; Pouderoijen, M. J.; Stouwdam, J. W.; Leclére, P. E. L. G.; Sijbesma, R. P.; Meijer, E. W.; Schenning, A. P. H. J. White-Light Emitting Hydrogen-Bonded Supramolecular Copolymers Based on π-Conjugated Oligomers. *J. Am. Chem. Soc.* **2008**, *131*, 833−843.

(22) Lei, J.; Ju, H. Signal Amplification Using Functional Nanomaterials for Biosensing. *Chem. Soc. Rev.* **2012**, *41*, 2122−2134.

(23) Farokhzad, O. C.; Langer, R. Impact of Nanotechnology on Drug Delivery. *ACS Nano* **2009**, *3*, 16−20.

(24) Zhang, Q.; Liu, K.; Nguyen, T.; Ma, X.; Wang, X.; Xing, B.; Zhao, Y. Multifunctional Mesoporous Silica Nanoparticles for Cancer-Targeted and Controlled Drug Delivery. *Adv. Funct. Mater.* **2012**, *22*, 5144−5156.

(25) Sen, T.; Sheppard, S. J.; Mercer, T.; Eizadi-Sharifabad, M.; Elhissi, A. Simple One-Pot Fabrication of Ultra-Stable Core-Shell Superparamagnetic Nanoparticles for Potential Application in Drug Delivery. *RSC Adv.* **2012**, *2*, 5221−5228.

(26) Bamrungsap, S.; Zhao, Z.; Chen, T.; Wang, L.; Li, C.; Fu, T.; Tan, W. Nanotechnology in Therapeutics. *Nanomedicine* **2012**, *7*, 1253−1271.

(27) Quinn, J. R.; Zimmerman, S. C. With Regard to the Hydrogen Bonding in Complexes of Pyridylureas, Less is More. A Role for Shape Complementarity and CH···O Interactions? *Org. Lett.* **2004**, *6*, 1649−1652.

(28) Yu, Y.; Tan, S.; Zhao, S.; Zhuang, X.; Song, Q.; Wang, Y.; Zhou, Q.; Zhang, Z. Antitumor Activity of Docetaxel-loaded Polymeric Nanoparticles Fabricated by Shirasu Porous Glass Membrane-Emulsification Technique. *Int. J. Nanomed.* **2013**, *8*, 2641−2652.
(29) Ma, D. L.; He, H. Z.; Leung, K. H.; Chan, D. S. H.; Leung, C. H. Bioactive Luminescent Transition-Metal Complexes for Biomedical Applications. *Angew. Chem., Int. Ed.* **2013**, *52*, 7666−7682.
(30) Lee, J. E.; Lee, N.; Kim, H.; Kim, J.; Choi, S. H.; Kim, J. H.; Kim, T.; Song, I. C.; Park, S. P.; Moon, W. K.; Hyeon, T. Uniform Mesoporous Dye-Doped Silica Nanoparticles Decorated with Multiple Magnetite Nanocrystals for Simultaneous Enhanced Magnetic Resonance Imaging, Fluorescence Imaging, and Drug Delivery. *J. Am. Chem. Soc.* **2010**, *132*, 552−557.
(31) Pramanik, M.; Chatterjee, N.; Das, S.; Saha, K. D.; Bhaumik, A. Anthracene-Bisphosphonate Based Novel Fluorescent Organic Nanoparticles Explored as Apoptosis Inducers of Cancer Cells. *Chem. Commun.* **2013**, *49*, 9461−9463.
(32) Noodleman, L.; Norman, J. G., Jr.; Osborne, J. H.; Aizman, A.; Case, D. A. Models for Ferredoxins: Electronic Structures of Iron-Sulfur Clusters with One, Two, and Four Iron Atoms. *J. Am. Chem. Soc.* **1985**, *107*, 3418−3426.
(33) Čejková, J.; Štěpánek, F. Compartmentalized and Internally Structured Particles for Drug Delivery-A Review. *Curr. Pharm. Des.* **2013**, *19*, 6298−6314.
(34) Leung, C. W. T.; Hong, Y. N.; Chen, S. J.; Zhao, E. G.; Lam, J. W. Y.; Tang, B. Z. A Photostable AIE Luminogen for Specific Mitochondrial Imaging and Tracking. *J. Am. Chem. Soc.* **2013**, *135*, 62−65.
(35) Chu, W.-J.; Chen, J.; Chen, C.-F.; Yang, Y.; Shuai, Z. Amidourea-based Hydrogen-Bonded Heteroduplexes: Structure and Assembling Selectivity. *J. Org. Chem.* **2012**, *77*, 7815−7822.
(36) Aida, T.; Meijer, E. W.; Stupp, S. I. Functional Supramolecular Polymers. *Science* **2012**, *335*, 813−817.
(37) Hong, Y.; Lam, J. W. Y.; Tang, B. Z. Aggregation-Induced Emission. *Chem. Soc. Rev.* **2011**, *40*, 5361−5388.
(38) Xu, Y. H.; Chen, L.; Guo, Z. Q.; Nagai, A.; Jiang, D. L. Light-Emitting Conjugated Polymers with Microporous Network Architecture: Interweaving Scaffold Promotes Electronic Conjugation, Facilitates Exciton Migration, and Improves Luminescence. *J. Am. Chem. Soc.* **2011**, *133*, 17622−17625.
(39) Bairi, P.; Roy, B.; Chakraborty, P.; Nandi, A. K. Co-Assembled White-Light-Emitting Hydrogel of Melamine. *ACS Appl. Mater. Interfaces* **2013**, *5*, 5478−5485.
(40) Shustova, N. B.; Cozzolino, A. F.; Dinca, M. Conformational Locking by Design: Relating Strain Energy with Luminescence and Stability in Rigid Metal−Organic Frameworks. *J. Am. Chem. Soc.* **2012**, *134*, 19596−19599.
(41) Yang, M.; McGovem, M. E.; Thompson, M. Genosensor Technology and the Detention of Interfacial Nucleic Acid Chemistry. *Anal. Chim. Acta* **1997**, *346*, 259−275.
(42) Ho, A. H.; Dore, K.; Boissinot, M.; Bergeron, M. G.; Tanguay, R. M.; Boudreau, D.; Leclerc, M. Direct Molecular Detection of Nucleic Acids by Fluorescence Signal Amplification. *J. Am. Chem. Soc.* **2005**, *127*, 12673−12676.
(43) Mondal, K.; Ali, M. A.; Agrawal, V. V.; Malhotra, B. D.; Sharma, A. Highly Sensitive Biofunctionalized Mesoporous Electrospun TiO_2 Nanofiber based Interface for Biosensing. *ACS Appl. Mater. Interfaces* **2014**, *6*, 2516−2527.
(44) Das, S. K.; Bhunia, M. K.; Chakraborty, D.; Khuda-Bukhsh, A. R.; Bhaumik, A. Hollow Spherical Mesoporous Phosphosilicate Nanoparticles as a Delivery Vehicle for an Antibiotic Drug. *Chem. Commun.* **2012**, *48*, 2891−2893.
(45) Fang, Y.; Zheng, G. F.; Yang, J. P.; Tang, H. S.; Zhang, Y. F.; Kong, B.; Lv, Y. Y.; Xu, C. J.; Asiri, A. M.; Zi, J.; Zhang, F.; Zhao, D. Y. Dual-Pore Mesoporous Carbon@Silica Composite Core−Shell Nanospheres for Multidrug Delivery. *Angew. Chem., Int. Ed.* **2014**, *53*, 5366−5370.
(46) Gomez-Crisostomo, N. P.; Lopez-Marure, R.; Zapata, E.; Zazueta, C.; Martinez-Abundis, E. Bax Induces Cytochrome c Release by Multiple Mechanisms in Mitochondria from MCF7 Cells. *J. Bioenerg. Biomembr.* **2013**, *45*, 441−448.